RADIATIVE PRECESSION OF AN ISOLATED NEUTRON STAR

A. Melatos[1,2,3]

Theoretical Astrophysics, Mail Code 130–33, California Institute of Technology,
Pasadena, CA 91125 USA

ABSTRACT

Euler's equations of motion are derived exactly for a rigid, triaxial, internally frictionless neutron star spinning down electromagnetically *in vacuo*. It is shown that the star precesses, but not freely: its regular precession relative to the principal axes of inertia couples to the component of the radiation torque associated with the near-zone radiation fields and is modified into an anharmonic wobble. The wobble period τ_1 typically satisfies $\tau_1 \lesssim 10^{-2}\tau_0$, where τ_0 is the braking time-scale; the wobble amplitude evolves towards a constant non-zero value, oscillates, or decreases to zero, depending on the degree of oblateness or prolateness of the star and its initial spin state; and the (negative) angular frequency derivative $\dot{\omega}$ oscillates as well, exhibiting quasi-periodic spikes for triaxial stars of a particular figure. In light of these properties, a young, Crab-like pulsar ought to display fractional changes of order unity in the space of a few years in its pulse profile, magnetic inclination angle, and $\dot{\omega}$. Such changes are not observed, implying that the wobble is damped rapidly by internal friction, if its amplitude is initially large upon crystallization of the stellar crust. If the friction is localized in the inner and outer crusts, the thermal luminosity of the neutron star increases by a minimum amount $\Delta L \approx 3 \times 10^{31}(\epsilon/10^{-12})(\omega/10^3\,\mathrm{rad\,s^{-1}})^2(\tau_\mathrm{d}/1\,\mathrm{yr})^{-1}\,\mathrm{erg\,s^{-1}}$, where ϵ is the ellipticity and τ_d is the damping time-scale, with the actual value of ΔL determined in part by the thermal conduction time τ_cond. The increased luminosity is potentially detectable as thermal X-rays lasting for a time $\approx \max(\tau_\mathrm{d}, \tau_\mathrm{cond})$ following crystallization of the crust.

Subject headings: pulsars — stars: neutron — stars: rotation

---

[1]Miller Fellow

[2]New address: Department of Astronomy, 601 Campbell Hall, University of California, Berkeley CA 94720 USA

[3]E-mail: melatos@astraea.berkeley.edu

1. INTRODUCTION

Does the angular momentum vector of an isolated neutron star change orientation as the star spins down? Early attempts to answer this question focused on the evolution of the angle α between the star's rotation and magnetic axes, which can be measured from pulsar polarization swings. Davis & Goldstein (1970) showed that α tends towards zero on the braking time-scale if the star is a rigid sphere or a fluid body in hydrostatic equilibrium — an unrealistic scenario which leaves all except the youngest pulsars as aligned rotators, contrary to observation. Goldreich (1970) observed that the crystalline crust of a neutron star supports shear stresses, thereby preventing a fraction of the hydrostatic bulge from aligning with the instantaneous rotation axis and establishing non-hydrostatic differences between the principal moments of inertia. In the absence of internal friction, such a triaxial star precesses about its principal axis with a period that is short compared to the braking time-scale, and the (fixed) angle between the principal axis and magnetic axis determines whether the precession amplitude (related to α) increases or decreases under the action of the braking torque (Goldreich 1970).

In reality, a neutron star is not internally frictionless. Elastic strain energy is dissipated in the crust as the non-hydrostatic deformation discussed above migrates around the star while it precesses (Goldreich 1970; Chau & Henriksen 1971; Macy 1974). There is also dissipation due to imperfect coupling between the differentially rotating crust and superfluid core (Shaham 1977; Alpar & Ögelman 1987; Link, Epstein & Baym 1993; Sedrakian, Wasserman & Cordes 1998). Both types of friction damp any precession that is initially present on a time-scale that is, theoretically, much shorter than the precession period — a plausible explanation for why the pulse profiles and polarization characteristics of young pulsars do not change secularly over several years as one expects if the precession is undamped. The only isolated neutron star unambiguously known to precess is PSR B1913+16 (Weisberg, Romani & Taylor 1989), where general relativistic effects are responsible. Tentative reports also exist of oscillatory variations in Crab and Vela timing residuals (e.g. Lyne, Pritchard & Smith 1988; McCulloch et al. 1990; Čadež, Galičič & Calvani 1997), and some authors have inferred changes in α on the braking time-scale from braking-index measurements (Allen & Horvath 1997; Link & Epstein 1997) and the evolution of pulsar radio beam statistics (Tauris & Manchester 1998).

The radiation torque acting on the neutron star has been treated in an incomplete fashion in all of the above work. The torque has two components: the familiar braking torque, responsible for the secular spin-down of the star, and a component associated with the inertia of the near-zone radiation fields, sometimes misleadingly termed the 'anomalous torque' (Good & Ng 1985), whose effect is to make a spherical star precess about its magnetic axis. In all analyses to date, either the total radiation torque has been set to zero, in order to study free precession (Macy 1974; Shaham 1977; Alpar & Ögelman 1987), or else the near-field component has been neglected, in the belief that it exerts no significant influence on the rotation (Davis & Goldstein 1970; Goldreich 1970; Chau & Henriksen 1971; Sedrakian et al. 1998). A careful study of both torque components in the context of a spherical star was carried out by Good & Ng (1985) for a magnetic dipole,

a magnetic quadrupole, and a hypothetical distribution of magnetospheric currents. Casini & Montemayor (1998) recently explored some effects of the near-field torque on a composite body with a spherically symmetric crust coupled to a spherical core (cf. de Campli 1980).

In this paper, we demonstrate that the near-field component of the radiation torque strongly influences the rotation of an internally frictionless neutron star. In Section 2, we derive and solve Euler's equations of motion for a rigid, triaxial magnet and show that the regular precession relative to the principal axes of inertia couples to the near-field torque, causing the star to wobble anharmonically. Certain potentially observable properties of the wobble are explored in Section 3, including its period and amplitude and the slow evolution of α and the angular frequency derivative $\dot{\omega}$. The results are applied to pulsar timing and polarization observations, and to the internal structure of young neutron stars, in Section 4.

2.   ROTATION OF A RIGID, TRIAXIAL NEUTRON STAR

In this section, the rotation of a rigid, triaxial body with an embedded magnetic dipole is treated analytically. Euler's equations of motion are written down in Section 2.1. Two key elements of the motion — the torque-driven radiative precession, and the inertial free precession — are discussed in Sections 2.2 and 2.3 respectively and their time-scales are identified. Euler's equations are then solved approximately in Section 2.4 by a time-averaging technique for the special case of a biaxial star. The similarities and differences between this treatment and previous work are noted in Section 2.5.

2.1.   Euler's Equations

Consider a rigid, triaxial star with principal axes $\mathbf{e}_1$, $\mathbf{e}_2$ and $\mathbf{e}_3$, corresponding principal moments of inertia I_1, I_2 and I_3, ellipticities $\epsilon = (I_3 - I_1)/I_1$ and $\epsilon' = (I_2 - I_1)/I_1$, and average radius r_0. We assume that the stellar magnetic field is dipolar and fixed in the star, and we restrict the magnetic axis $\mathbf{m}$ to lie in the plane spanned by $\mathbf{e}_1$ and $\mathbf{e}_3$, at an angle χ to $\mathbf{e}_3$; this entails a slight loss of generality. We also assume that the star is internally frictionless and that it rotates *in vacuo*, so that it is unaffected by magnetospheric currents; refer to Goldreich (1970) and Melatos (1997) for justifications of the latter assumption. It is important to keep in mind that, although we idealize the star as a rigid body for simplicity, in reality the ellipsoid of inertia is determined by an equilibrium between elastic and hydromagnetic forces, as discussed in Section 2.3.

In Appendix A, we evaluate the radiation torque acting on the star from the electromagnetic fields generated by a magnetized, conducting sphere rotating *in vacuo* (Deutsch 1955; Melatos 1997); it is assumed that the star's triaxiality can be neglected when calculating the fields and torque. Upon resolving the torque into components along the principal axes, we arrive at Euler's

equations of motion,

$$\dot{u}_1 = (\epsilon' - \epsilon)u_2 u_3 + (\omega_0\tau_0)^{-1}\cos\chi\left[u^2 F(x_0)(-u_1\cos\chi + u_3\sin\chi)\right.$$
$$\left. + uG(x_0)u_2(u_1\sin\chi + u_3\cos\chi)\right], \tag{1}$$

$$(1+\epsilon')\dot{u}_2 = \epsilon u_1 u_3 + (\omega_0\tau_0)^{-1}\left[-u^2 F(x_0)u_2\right.$$
$$\left. + uG(x_0)(-u_1\cos\chi + u_3\sin\chi)(u_1\sin\chi + u_3\cos\chi)\right], \tag{2}$$

$$(1+\epsilon)\dot{u}_3 = -\epsilon' u_1 u_2 - (\omega_0\tau_0)^{-1}\sin\chi\left[u^2 F(x_0)(-u_1\cos\chi + u_3\sin\chi)\right.$$
$$\left. + uG(x_0)u_2(u_1\sin\chi + u_3\cos\chi)\right], \tag{3}$$

with

$$F(x_0) = \frac{x_0^4}{5(x_0^6 - 3x_0^4 + 36)} + \frac{1}{3(x_0^2 + 1)}, \tag{4}$$

$$G(x_0) = \frac{3(x_0^2 + 6)}{5x_0(x_0^6 - 3x_0^4 + 36)} + \frac{3 - 2x_0^2}{15x_0(x_0^2 + 1)}. \tag{5}$$

In equations (1) to (5), ω_0 is the magnitude of the angular velocity vector $\boldsymbol{\omega}(t)$ at time $t = 0$, we define dimensionless variables $\mathbf{u} = \boldsymbol{\omega}/\omega_0$ and $x_0 = (r_0\omega_0/c)u$, an overdot denotes differentiation with respect to the dimensionless time coordinate $s = \omega_0 t$, and

$$\tau_0 = \frac{\mu_0 c^3 I_1}{2\pi B_0^2 r_0^6 \omega_0^2} \tag{6}$$

is the characteristic braking time-scale at $t = 0$, in terms of the magnetic field strength B_0 at the magnetic poles (Deutsch 1955).

The form factors $F(x_0)$ and $G(x_0)$ reflect the structure of the near-zone radiation fields through their dependences on x_0. The familiar braking torque, which is responsible for the secular spin-down of the star, is associated with terms proportional to $F(x_0)$, whereas the near-field torque discussed in Section 1 is associated with terms proportional to $G(x_0)$. In most applications, r_0 is taken to be the stellar radius R (cf. Section 3.6 and Kaburaki 1981, Melatos 1997), yielding $x_0 \ll 1$, $F(x_0) = 1/3$ and $G(x_0) = 3/10x_0$. The near-field torque is therefore much greater than the braking torque in this regime and acts on a commensurately shorter time-scale. Equations (4) and (5) differ from the expressions $F(x_0) = 1/3$ and $G(x_0) = 1/2x_0$ found in previous works (Davis & Goldstein 1970; Goldreich 1970), partly because the treatment in this paper is not restricted to $x_0 \ll 1$, and partly because we model the star's internal magnetization in a slightly different way, as explained in Appendix A.

2.2. Radiative Precession

The near-field component of the radiation torque causes the star to precess and nutate about its magnetic axis. We call this motion 'radiative precession'. To understand its origin, consider the

simple special case of a spherical star ($\epsilon = \epsilon' = 0$). In the regime $x_0 \ll 1$, where the form factor $uG(x_0) \approx 3c/10r_0\omega_0$ is independent of s, Euler's equations (1) to (3) have the exact solution (cf. Davis & Goldstein 1970)

$$u_1 \;=\; u_{1,0}u_{3,0} \left\{ \exp\left[\frac{2u_{3,0}^2 F(x_0)s}{\omega_0\tau_0} \right] - u_{1,0}^2 \right\}^{-1/2} \cos\left[\frac{u_{3,0}uG(x_0)s}{\omega_0\tau_0} \right], \tag{7}$$

$$u_2 \;=\; u_{1,0}u_{3,0} \left\{ \exp\left[\frac{2u_{3,0}^2 F(x_0)s}{\omega_0\tau_0} \right] - u_{1,0}^2 \right\}^{-1/2} \sin\left[\frac{u_{3,0}uG(x_0)s}{\omega_0\tau_0} \right], \tag{8}$$

$$u_3 \;=\; u_{3,0} \;, \tag{9}$$

for the initial conditions $u_1 = u_{1,0}$, $u_2 = 0$, $u_3 = u_{3,0} \neq 0$ at $s = 0$.[4] A spherical star therefore precesses harmonically about $\mathbf{m}$ with period

$$\tau_1 = \left(\frac{20\pi r_0 \omega_0}{3u_{3,0}c} \right) \tau_0 \ll \tau_0 \;, \tag{10}$$

and the precession amplitude decays exponentially on the time-scale $3\tau_0/u_{3,0}^2$, as $\boldsymbol{\omega}$ aligns with $\mathbf{m}$. Taking $r_0 = R = 10\,\mathrm{km}$ (cf. Section 3.6) and $I_1 = 1 \times 10^{38}\,\mathrm{kg\,m^2}$, we obtain numerically

$$\tau_1 = 4 \times 10^{13} \left(\frac{B_0}{10^8\,\mathrm{T}} \right)^{-2} \left(\frac{\omega}{1\,\mathrm{rad\,s^{-1}}} \right)^{-1} \mathrm{s} \;, \tag{11}$$

which is to be compared with

$$\tau_0 = 5 \times 10^{16} \left(\frac{B_0}{10^8\,\mathrm{T}} \right)^{-2} \left(\frac{\omega}{1\,\mathrm{rad\,s^{-1}}} \right)^{-2} \mathrm{s} \;. \tag{12}$$

Radiative precession occurs due to the asymmetric inertia of the near-zone radiation fields of a rotating magnetic dipole (Goldreich 1970): the electromagnetic energy density $\mathcal{E}$ is greater at the magnetic poles ($\mathcal{E} \approx B_0^2/2\mu_0$) than at the magnetic equator ($\mathcal{E} \approx B_0^2/8\mu_0$), translating into a fractional distortion $\epsilon^{\mathrm{rad}} \approx (\delta\mathcal{E}/c^2)r_0^5/I_1$ of the moment of inertia about $\mathbf{m}$. The effect depends only on the radiation fields outside the star, which in turn are determined completely by the magnetic field at the stellar surface and the property that the star is a good conductor (Deutsch 1955). The magnetic field inside the star does not influence the radiative precession.

The near-field torque contributes terms proportional to u_2u_3 and u_1u_3 in (1) and (2) respectively and therefore adds to, or subtracts from, similar terms arising from material distortions (i.e. ϵ and ϵ'). Thus a biaxial star ($\epsilon' = 0$) with $\chi = 0$ and $\epsilon = \epsilon^{\mathrm{rad}}$ does not precess at all, because the terms $(\epsilon' - \epsilon)u_2u_3$ and ϵu_1u_3 are cancelled out exactly by the near-field torque.

---

[4]See Davis & Goldstein (1970) for a discussion of the singular special case $u_{3,0} = 0$.

2.3. Free Precession

In the absence of the radiation torque, a triaxial neutron star precesses relative to its principal axes of inertia on a time-scale $\tau_2 = 2\pi/\epsilon\omega$, where ϵ is the non-hydrostatic ellipticity. A variety of non-hydrostatic mechanisms, many with geological analogues (Lambeck 1980), combine to deform the stellar mass distribution. We concentrate on elastic and magnetic deformations in this paper.

The crystalline stellar crust supports shear stresses which prevent a fraction of the hydrostatic bulge from aligning with the instantaneous rotation axis. For a crust with uniform shear modulus μ, one finds $\epsilon^{\mathrm{cr}} = 5\tilde{\mu}\omega^2 R^3/4(1 + \tilde{\mu})GM$, with $\tilde{\mu} = 38\pi\mu R^4/3GM^2$, where M is the mass of the star (Goldreich 1970; Lambeck 1980, p. 42). This elastic deformation yields a precession period

$$\tau_2^{\mathrm{cr}} = 1 \times 10^{14} \left(\frac{\mu}{10^{28}\,\mathrm{N\,m^{-2}}} \right)^{-1} \left(\frac{\omega}{1\,\mathrm{rad\,s^{-1}}} \right)^{-3}\,\mathrm{s} \tag{13}$$

for neutron star parameters. If the crust is structured as a Coulomb lattice, one has $\tilde{\mu} \lesssim 10^{-4}$ and the non-hydrostatic fraction of the bulge is small; however, the exact value of $\tilde{\mu}$ is uncertain and may be much less than this upper bound.

The magnetic field inside the star creates an additional deformation because non-radial field gradients (e.g. between the poles and equator if the field is a dipole) support non-radial matter-density gradients in hydromagnetic equilibrium. (This is not related in any way to the electromagnetic inertia of the external radiation fields discussed in Section 2.2.) The geometry and magnitude of the deformation is difficult to estimate, because little is known about the structure of the internal magnetic field. Thompson & Duncan (1993) argued that, if the internal field is generated after collapse in a convective dynamo, then it must be organized into randomly oriented loops $\sim 1\,\mathrm{km}$ in size, each with field strength $\sim 10^{11}$ T; the neutron star rotates too slowly (Rossby number Ro $\gtrsim 10$) to establish a coherent toroidal field at the base of the convection zone (cf. the Solar dynamo). On the other hand, if the internal field is generated before collapse in the progenitor star (e.g. in the convective outer envelope or hydrogen-burning core), a large toroidal field can grow (Ro $\lesssim 0.1$). Blandford, Applegate & Hernquist (1983) examined toroidal field generation by a thermoelectric dynamo. Several authors have raised the possibility of a very strong internal field ($\gtrsim 10^{10}$ T $\gg B_0$) in diverse contexts, including off-centred-dipole theories of the pulsar death line (Arons 1998), thermally regulated resurrection of a buried field (Muslimov & Page 1996), Ohmic decay in an anisotropically conducting core (Haensel, Urpin & Yakovlev 1990), crust-core coupling in Vela glitches (Abney, Epstein & Olinto 1996; cf. Easson 1979), and the effect of a virial field (10^{14} T) on modified Urca cooling (Yuan & Zhang 1998) and the quark-hadron equation of state (Pal, Bandyopadhyay & Chakrabarty 1998).

Assuming that the internal magnetic field is at least as strong as the surface field and roughly dipolar, we find that the hydromagnetic deformation satisfies $\epsilon^{\mathrm{mag}} \gtrsim \epsilon^{\mathrm{rad}}c^2/c_{\mathrm{s}}^2$, where c_{s} is the isothermal sound speed ($= 3^{-1/2}c$ in a relativistic star); in other words, ϵ^{mag} exceeds ϵ^{rad} at least by a factor of order the ratio of the stellar to Schwarzschild radii. This yields an upper bound on

the precession period τ_2^{mag} associated with the hydromagnetic deformation given by

$$\tau_2^{\mathrm{mag}} \leq 1 \times 10^{13} \left(\frac{B_0}{10^8 \,\mathrm{T}}\right)^{-2} \left(\frac{\omega}{1 \,\mathrm{rad\,s^{-1}}}\right)^{-1} \mathrm{s} \; . \tag{14}$$

Note that the combined elasto-hydromagnetic deformation is triaxial in general. Biaxiality ($\epsilon' = 0$) is a good approximation only when one has $\epsilon^{\mathrm{cr}} \ll \epsilon^{\mathrm{mag}}$ (or else $\epsilon^{\mathrm{cr}} \gg \epsilon^{\mathrm{mag}}$) and the internal magnetic field (or crust) is symmetric about a unique axis.

Equations (11), (13) and (14) reveal that, as a rule, *the periods of the radiative precession and free precession are comparable.* One has $\tau_1 \sim \tau_2^{\mathrm{mag}}$, if the internal and surface magnetic fields are of similar magnitude, and sometimes $\tau_1 \sim \tau_2^{\mathrm{cr}}$ as well, e.g. for a one-second pulsar with $\mu = 10^{28} \,\mathrm{N\,m^{-2}}$ and $B_0 = 4 \times 10^8 \,\mathrm{T}$. In general, therefore, the 'free' precession is not free at all; rather, it couples to the near-field component of the radiation torque, and its character is modified significantly as a result. This coupling has been overlooked in the literature on aspherical rotators to date (Goldreich 1970; Chau & Henriksen 1971; Macy 1974; Shaham 1977; Alpar & Ögelman 1987; Sedrakian et al. 1998), and the remainder of this paper is devoted to exploring its consequences. It can only be neglected under certain circumstances, e.g. when the internal magnetic field is strong and the free precession is therefore fast ($\tau_2^{\mathrm{mag}} \lesssim 0.05\tau_1$; see Section 3.2).

2.4. Separating the Braking and Precession Time-Scales: An Approximate Solution of Euler's Equations

Euler's equations (1) to (3) can be solved approximately by averaging over the precession period, exploiting the fact that both τ_1 and τ_2 are small compared to τ_0 (except in the regime $x_0 \sim 1$; see Section 3.6). The analysis parallels that by Goldreich (1970), with one crucial difference: we account fully for the radiative precession in what follows, whereas Goldreich (1970) artificially suppressed it by averaging the braking torque *and near-field torque* over the free precession period.

Let us restrict attention to a biaxial star ($\epsilon' = 0$) for the sake of simplicity. When the 'slow' braking terms in Euler's equations, proportional to $(\omega_0\tau_0)^{-1}F(x_0)$, are neglected relative to 'fast' terms, proportional to ϵ and $(\omega_0\tau_0)^{-1}uG(x_0)$, the equations reduce to the zeroth-order system

$$\dot{u}_1 = \epsilon\beta^{-1}u_2[u_1 \sin\chi \cos\chi - (\beta - \cos^2\chi)u_3], \tag{15}$$

$$\dot{u}_2 = \epsilon\beta^{-1}[(u_3^2 - u_1^2)\sin\chi \cos\chi + (\beta - \cos^2\chi + \sin^2\chi)u_1u_3], \tag{16}$$

$$\dot{u}_3 = -\epsilon\beta^{-1}u_2(u_1 \sin\chi + u_3 \cos\chi)\sin\chi, \tag{17}$$

with

$$\beta = \frac{\epsilon\omega_0\tau_0}{uG(x_0)} \; . \tag{18}$$

The parameter β is independent of s in the regime $x_0 \ll 1$ and is positive or negative according to whether the star is oblate or prolate. Upon multiplying (15), (16) and (17) by u_1, u_2 and u_3

respectively, we find that

$$\eta = u_1^2 + u_2^2 + u_3^2 \tag{19}$$

is a constant of the motion; in other words, the total angular momentum of the star is unaffected by the near-field component of the radiation torque. Furthermore, dividing (15) by (17) yields a second constant of the motion

$$\gamma = (u_1 \sin \chi + u_3 \cos \chi)^2 - \beta u_3^2 \ , \tag{20}$$

which loosely measures the difference between the precession and magnetic inclination angles. One can solve (16), (19) and (20) simultaneously to obtain a first-order differential equation for u_2, solvable by quadrature, whose solution is exactly periodic but anharmonic in general. For the illustrative special case $\chi = 90°$, $\beta > 0$ calculated in Appendix B, we find

$$u_1 = \left(\frac{\gamma + \eta\beta}{\beta + 1}\right)^{1/2} \mathrm{cn}\left[\epsilon\left(\frac{\eta - \gamma}{\beta}\right)^{1/2} s + \Phi\right], \tag{21}$$

$$u_2 = \left(\frac{\gamma + \eta\beta}{\beta}\right)^{1/2} \mathrm{sn}\left[\epsilon\left(\frac{\eta - \gamma}{\beta}\right)^{1/2} s + \Phi\right], \tag{22}$$

$$u_3 = \left(\frac{\eta - \gamma}{\beta + 1}\right)^{1/2} \mathrm{dn}\left[\epsilon\left(\frac{\eta - \gamma}{\beta}\right)^{1/2} s + \Phi\right], \tag{23}$$

where sn, cn and dn are Jacobian elliptic functions with modulus $k^2 = (\gamma + \eta\beta)/(\eta - \gamma)\beta$. Note that the phase Φ of the oscillation is a third constant of the motion, related to u_1, u_2 and u_3 in a complicated way.

When terms proportional to $(\omega_0 \tau_0)^{-1} F(x_0)$ are restored to Euler's equations, the above solutions remain approximately valid, but the constants of the motion are converted into slowly varying functions of s, viz., $\eta = \eta(s)$, $\gamma = \gamma(s)$ and $\Phi = \Phi(s)$. The slow variation occurs on the braking time-scale τ_0, which is long compared to $\tau_1 \sim \tau_2 \sim \epsilon^{-1}$. Analytic expressions for $\dot{\eta}$, $\dot{\gamma}$ and $\dot{\Phi}$ are obtained by substituting (21), (22) and (23) into (1), (2) and (3) and averaging over Φ. Results for $\chi = 90°$ are given for reference in Appendix B.

2.5. Comparison with Previous Work

Equations (1) to (3) reduce to the equations solved by Davis & Goldstein (1970) for the special case of a spherical star ($\epsilon = \epsilon' = 0$, and hence $\chi = 0$ without loss of generality), and to those solved by Goldreich (1970) in the regime $\tau_2 \ll \tau_1$ where the free precession is much faster than the radiative precession. The latter regime corresponds to a large elasto-hydromagnetic deformation, such as when the internal magnetic field is much stronger than the surface field (see Section 2.3), but it is not fully general. In contrast, the solutions presented in Section 2.4 and the numerical results in Section 3 address the general problem where τ_1/τ_2 is arbitrary, including the regime $\tau_1 \approx \tau_2$ where the free and radiative precessions couple together. Previous authors have

discussed the physical origins of τ_1 and τ_2 (Goldreich 1970; Chau & Henriksen 1971; de Campli 1980).

Our analysis cannot be compared directly with previous work treating the star as anelastic (e.g. Macy 1974) or with models featuring a core and crust coupled together (Shaham 1977; de Campli 1980; Alpar & Ögelman 1987; Casini & Montemayor 1998; Sedrakian et al. 1998).

3. PROPERTIES OF THE ROTATION

The motion analyzed in Section 2 is characterized by several properties of potential observational significance which we now investigate, including the precession period (Section 3.1) and amplitude (Section 3.2), the evolution of the magnetic inclination (Section 3.3), the different behaviour of oblate and prolate stars (Section 3.4), the phenomenon of 'pseudo-glitches' in $\dot{\omega}$ (Section 3.5), and the effect of a corotating magnetosphere (Section 3.6). In what follows, we assume that the orientation of $\boldsymbol{\omega}$ is arbitrary at the time when the neutron star first crystallizes into an object with a rigid crust spinning down electromagnetically. In other words, $u_{1,0}$, $u_{2,0}$ and $u_{3,0}$ are assumed to be comparable; we do not choose a privileged initial spin state where $\boldsymbol{\omega}$ is parallel to one of the principal axes. This assumption is important because in Section 4 we present strong observational evidence that isolated pulsars evolve rapidly towards a stable state of this sort, probably under the action of internal friction. Consequently, the properties investigated below characterize neutron stars early in their lives.

The results in this section are mainly presented in the context of a biaxial star ($\epsilon' = 0$) for two reasons. First, we find numerically that the rotation properties of biaxial and triaxial stars are qualitatively alike, except for pseudo-glitches (Section 3.5) which are an intrinsically triaxial phenomenon. Second, the aim of this section is to illustrate those aspects of the dynamics that are observationally relevant; an exhaustive quantitative survey of the rotation of a triaxial magnet lies outside the scope of this paper. Formally speaking, however, biaxiality is a good approximation only as long as one has $\epsilon^{\mathrm{cr}} \ll \epsilon^{\mathrm{mag}}$ (or else $\epsilon^{\mathrm{cr}} \gg \epsilon^{\mathrm{mag}}$) and the internal magnetic field (or crust) is symmetric about a unique axis.

3.1. Precession Period

The period Δs of the anharmonic precession is typically $\sim |\beta|^{1/2} |\epsilon|^{-1}$, in units of ω_0^{-1}. For the special case $\chi = 90°$, $\beta > 0$, Δs is given exactly by

$$\Delta s = \frac{4}{|\epsilon|} \left(\frac{\beta}{\eta - \gamma} \right)^{1/2} K \left\{ \left[\frac{\gamma + \eta\beta}{\beta(\eta - \gamma)} \right]^{1/2} \right\}, \tag{24}$$

where $K(k)$, a complete elliptic integral of the first kind, increases logarithmically from $K(0) = \pi/2$ to $K(1) = \infty$. Note that the precession is not exactly periodic, because $\Delta s \propto (\eta - \gamma)^{-1/2}$ increases

adiabatically on the braking time-scale τ_0. Indeed, Δs increases significantly and approaches $\omega_0 \tau_0$ (so that the separation into slow and fast time-scales in Section 2.4 breaks down) under two special sets of circumstances: (i) at $k = 1$, where u_1, u_2 and u_3 suddenly swap oscillation modes ('mode jumping'; see Section 3.4); and (ii) at the $\eta = \gamma$ resonance, where the the star rotates steadily with $u_2 = u_3 = 0$ and $u_1 = $ const for $\beta > -1$ (Section 3.4). If the star is triaxial, a second precession time-scale, $\Delta s \sim |\beta|^{1/2} |\epsilon'|^{-1}$, is introduced.

3.2. Precession and Nutation Amplitudes

Figure 1 displays the precession angle θ, defined to be the angle between $\boldsymbol{\omega}$ and $\mathbf{e}_3$ ($\cos\theta = u_3/u$), as a function of time. We see from Figure 1 that the star precesses ($\theta \neq 0$ on average) and nutates (θ oscillates in a range $\theta_1 \leq \theta \leq \theta_2$ during one precession period), and that the slow evolution of the precession and nutation amplitudes is determined by β, χ and the initial orientation of $\boldsymbol{\omega}$. In the regime $\beta \gg 1$ where the free precession period τ_2 is shorter than both torque-related time-scales τ_0 and τ_1, the nutation amplitude is small and θ decreases exponentially to zero for $\chi = 20°$ (thick band in Figure 1). This result, and a similar calculation for $\chi = 70°$ (not shown), confirm Goldreich's (1970) conclusion that the slow evolution of θ in the regime $\beta \gg 1$ depends solely on χ, with $\theta \to 0°$ for $\chi < \chi_{\rm cr} = \cos^{-1}(3^{-1/2}) \approx 55°$ and $\theta \to 90°$ for $\chi > \chi_{\rm cr}$.

Goldreich's (1970) conclusion is invalid when τ_1 and τ_2 are comparable. The solid and dotted curves in Figure 1 both correspond to $\chi = 20° < \chi_{\rm cr}$, but with $\beta = 0.8$ and hence $\tau_1 \sim \tau_2$. Neither curve behaves as predicted by Goldreich (1970): either θ approaches a constant non-zero value while the nutation amplitude decreases to zero (solid curve), or else θ remains constant on average with a peak-to-peak nutation amplitude of $\approx 50°$ (dotted curve). In each case, *the precession is persistent*, and its character is determined by the initial orientation of $\boldsymbol{\omega}$.

3.3. Do the Magnetic and Rotation Axes Align?

The magnetic inclination angle α between $\boldsymbol{\omega}$ and $\mathbf{m}$ is defined in terms of u_1, u_2 and u_3 by $u\cos\alpha = u_1 \sin\chi + u_3 \cos\chi$. In Figure 2, we plot α as a function of time for several choices of β and χ. For $\chi = 0°$, $\beta = 0.5$, we see that α decreases exponentially to zero on the braking time-scale. By solving (1) to (3) analytically for $\chi = 0°$, one can show that α approaches zero for arbitrary β, implying that a star subject to a predominantly magnetic deformation ultimately becomes an aligned rotator — a state in which it cannot be detected as a pulsar. An aligned final state ($\alpha = 180°$) can also be attained by a star with $\chi \neq 0°$ (upper dotted curve in Figure 2). In contrast, if the star nutates persistently as discussed in Section 3.2, α mimics θ and oscillates within a range (typically tens of degrees).

3.4. Oblate and Prolate Stars, and the η-γ Phase Plane

An instructive way to view the evolution of the rotation is to follow the star's trajectory $[\eta(s), \gamma(s)]$ on the η-γ phase plane. As shown in Section 2.4, η and γ are approximately constant over one precession period, varying slowly on the braking time-scale τ_0. Figure 3 shows phase diagrams for three stars with $\chi = 90°$ and different ellipticities. Since η and γ are not exactly constant over one precession period, the trajectories are slightly irregular.

Figure 3(a) shows that an *oblate* star ($\beta > 0$) evolves asymptotically towards a state with $\gamma = \eta \neq 0$ and hence $u_2 = u_3 = 0$, $u_1 = \mathrm{const}$ (see [19] and [20]); in other words, for $\chi = 90°$, an oblate star always approaches steady-state rotation with $\boldsymbol{\omega}$ parallel to $\mathbf{m}$ ($= \mathbf{e}_1$). Equations (1) to (3) imply that this is a singular fixed point which exists for $\chi = 90°$ only. The evolution of a *prolate* star ($\beta < 0$) depends on the relative magnitudes of the precession periods τ_1 (radiative) and τ_2 (free). When the radiative precession is faster ($-1 < \beta < 0$), as in Figure 3(b), the star evolves to a state with $\gamma = \eta \neq 0$, as discussed above. When the free precession is faster ($\beta < -1$), as in Figure 3(c), the star evolves to a state with $\gamma = \eta = 0$, and $\boldsymbol{\omega}$ does not necessarily align with any preferred axis on the way, although it may do so for specific initial conditions. In all the above cases, the phase-plane trajectories are confined within the triangular region $0 \leq \eta \leq 1$, $\min(-\eta\beta, 0) \leq \gamma \leq \max(\eta, -\eta\beta)$.

How are the phase diagrams modified for $\chi \neq 90°$? Firstly, the trajectories are confined to a smaller (larger) triangular region for $\beta > 0$ ($\beta < 0$) defined by

$$0 \leq \eta \leq 1, \qquad \min(0, \gamma_1, \gamma_3) \leq \gamma \leq \max(\gamma_1, \gamma_2, \gamma_3), \tag{25}$$

with $\gamma_1 = \eta(\cos^2 \chi - \beta)$, $\gamma_2 = \eta \sin^2 \chi$ and

$$\gamma_3 = \eta[\sin^2(\chi + \psi) - \beta \sin^2 \psi], \qquad \tan 2\psi = \frac{\sin 2\chi}{\beta - \cos 2\chi}. \tag{26}$$

Secondly, although the $\beta > -1$ trajectories approach the diagonal line $\gamma = \max(\gamma_1, \gamma_2, \gamma_3)$, they do not stop there like in Figure 3. Instead, they bend downwards to merge with the diagonal, travelling down along it as η decreases. This is because the state $\gamma = \max(\gamma_1, \gamma_2, \gamma_3)$ is only a fixed point for $\chi = 90°$, as pointed out above.

The trajectories in Figures 3(a)–(c) asymptotically approach, or travel exactly along, the lines $\gamma = \eta$ and $\gamma = -\eta\beta$ except in the case $-1 < \beta < 0$ (Figure 3[b]), where trajectories with $\gamma < -\beta$ at $s = 0$ subsequently cross the line $\gamma = -\eta\beta$. When this happens, a phenomenon we call 'mode jumping' takes place. As shown in Figure 4, u_1 and u_2 interchange oscillation modes at $s \approx 2.7\,\omega_0\tau_0$, swapping between a wine-glass mode and a sinusoidal mode, while the u_3 oscillation becomes temporarily flatter-peaked.

3.5.   Pseudo-Glitches in the Frequency Derivative of a Triaxial Star

A triaxial ellipsoid of inertia arises naturally if, for example, the deformation is predominantly magnetic with appreciable quadrupolar and off-centred components, or if one has $\epsilon^{\rm cr} \sim \epsilon^{\rm mag}$. Figure 5 plots the angular frequency derivative $\dot{u}$ as a function of time for a triaxial star with $\epsilon' = 0.09\epsilon$. We see that the smooth, braking-related decrease of $|\dot{u}|$ is punctuated by sudden, quasi-periodic spikes in which $|\dot{u}|$ changes by up to 90 per cent. We call these excursions 'pseudo-glitches'. They resemble true glitches because (i) they recur quasi-periodically with period $\sim x_0\tau_0$ ($\approx 10\,{\rm yr}$ for the Crab), and (ii) $\dot{u}$ returns to its trend value after each excursion. However, they are manifestly not true glitches because (i) their rise time is too long (cf. $\lesssim 10^{-10}\tau_0$ for Crab glitches), and (ii) they do not cause u itself to increase. Note that $\dot{u}$ oscillates about the average spin-down trend even for $\epsilon' = 0$, but not in the spiky fashion of Figure 5.

What is the physical origin of pseudo-glitches? The dotted curve in Figure 5 shows that pseudo-glitches coincide with rapid changes in α, accompanied by mode jumping, which occur when the free precession is modulated on a fast time-scale $(\epsilon'/\epsilon)\tau_2$ which couples resonantly to the radiative precession (i.e. $\epsilon\tau_1 \approx \epsilon'\tau_2$). It turns out that the sharpness of the spikes is sensitive to ϵ' and $uG(x_0)$; for the example in Figure 5, the spikes are washed out once ϵ' falls outside the range $0.05 \lesssim \epsilon'/\epsilon \lesssim 0.15$. Figure 5 shows the case $\chi = 40°$. For larger χ, the small bumps between the spikes increase in amplitude until they become spiky themselves. For smaller χ, the bumps flatten until they disappear.

3.6.   Corotating Magnetosphere

The foregoing results pertain to the regime $x_0 \ll 1$, where r_0 is taken to be the stellar radius R. However, recent work by Melatos (1997) suggests that the corotating magnetosphere of a neutron star acts as a perfectly conducting, rigid extension of the stellar interior out to a characteristic radius $r_{\rm v}$ where outflowing plasma is not constrained to flow along magnetic field lines by cyclotron losses, and that it is therefore necessary to set $r_0 = r_{\rm v}$ when calculating electromagnetic spin-down properties like pulsar braking indices. For young pulsars (e.g. the Crab, PSR B1509−58, PSR B0540−69), one finds $r_{\rm v} \lesssim c/\omega$, and hence $x_0 \lesssim 1$.

In the regime $x_0 \lesssim 1$, the radiative precession period satisfies $\tau_1 \sim \tau_0$, the near-field radiation torque uncouples from the free precession, and the evolution of the precession amplitude is governed completely by $\chi/\chi_{\rm cr}$ (Goldreich 1970). However, a pulsar born with $x_0 \lesssim 1$ soon evolves towards the regime $x_0 \ll 1$ as ω decreases. Therefore, unless the free precession amplitude decreases to zero during the initial braking phase with $x_0 \lesssim 1$ (*not* the outcome in general), the rotation behaves thereafter in the way described in Sections 3.1 to 3.5.

4. APPLICATION TO OBSERVATIONS

Timing and polarization studies suggest that most, if not all, young pulsars do not precess in the manner described in Sections 2 and 3. The implication is that isolated neutron stars born with a large precessional motion approach stable spin states ($\boldsymbol{\omega}$ parallel to a principal axis of inertia) over times that are short compared to their current ages, probably due to internal friction. We outline the conditions for a neutron star to be born with a large precessional motion in Section 4.1, summarize the status of observational searches for precession in Section 4.2, and discuss the observational consequences of frictional stabilization in Section 4.3.

4.1. Precession at Birth

When a neutron star is born, it spins about an axis $\boldsymbol{\omega}_0$ dictated by conservation of angular momentum (of the degenerate remnant and the ejecta) during the supernova explosion. There is no reason why $\boldsymbol{\omega}_0$ should immediately be parallel to the principal axis of greatest non-hydrostatic moment of inertia (the magnetic axis $\mathbf{m}$, since the star is a fluid). Indeed, Thompson & Duncan (1993) argued that post-collapse convection destroys any correlation between $\boldsymbol{\omega}_0$ and $\mathbf{m}$.

Viscous dissipation in the fluid star forces $\boldsymbol{\omega}_0$ to approach $\mathbf{m}$ over time. The dissipation rate is therefore critical in determining whether the star will exhibit a large initial precession when its crust crystallizes. Unfortunately, the viscosity of a newly born neutron star is poorly constrained. Cutler & Lindblom (1987) estimate the viscous damping time (e.g. for stellar oscillations) to be roughly $3 \times 10^2 (\rho/10^{17}\,\mathrm{kg\,m^{-3}})^{-1.25}(T/10^9\,\mathrm{K})^2$yr, to be compared with a crust crystallization time of less than one year, but this estimate is known to be valid only in narrow ranges of density ρ and temperature T centred on the above fiducial values. In what follows, we make no assumption about the viscous damping time and instead explore several possible scenarios.

If the viscosity is high enough, $\boldsymbol{\omega}_0$ aligns with $\mathbf{m}$ first, before the crust crystallizes. Assuming that the symmetry axis of the crust when it crystallizes is along $\boldsymbol{\omega}_0$ (likely, though not certain), then the principal axis $\mathbf{e}_3$ (from both elastic and magnetic contributions) is parallel to $\boldsymbol{\omega}_0$, and there is no precession.

If the viscosity is low enough, the crust crystallizes first, before $\boldsymbol{\omega}_0$ has time to align with $\mathbf{m}$ — the order of events implied by the viscosity estimates of Cutler & Lindblom (1987). In this scenario, two things can happen: (i) one has $\epsilon^{\mathrm{cr}} \gg \epsilon^{\mathrm{mag}}$, and the symmetry axis of the crust when it crystallizes is along $\boldsymbol{\omega}_0$, so that $\mathbf{e}_3$ is parallel to $\boldsymbol{\omega}_0$ and there is no precession; or (ii) one has $\epsilon^{\mathrm{cr}} \ll \epsilon^{\mathrm{mag}}$, so that $\mathbf{e}_3$ is parallel to $\mathbf{m}$ — which is *not* parallel to $\boldsymbol{\omega}_0$ at the epoch of crystallization — and there is a large precession. Below we explore the observational implications of scenario (ii).

4.2. Changes in Pulse Profile and Polarization

The results of Section 3 imply that a neutron star in an arbitrary initial spin state precesses (and nutates) with period $\sim x_0\tau_0$ and a typical amplitude of tens of degrees, and that the motion is persistent in general. One therefore expects fractional changes of order unity in the pulse profile (e.g. relative height or separation of conal components), magnetic inclination angle α (measured from polarization-swing data), and angular frequency derivative $\dot{\omega}$ (measured by timing) over a single precession period. For young, Crab-like objects ($x_0 \approx 10^{-2}$, $\tau_0 \approx 10^3\,$yr), the fractional changes amount to ~ 10 per cent per year and ought to be readily observable; for old objects ($x_0 \approx 10^{-3}$, $\tau_0 \approx 10^6\,$yr), the changes amount to ~ 0.1 per cent per year and are harder to detect.

Contrary to the above expectation, the only reliable detection of neutron-star precession to date has been Weisberg et al.'s (1989) discovery of the general relativistic geodetic precession of PSR 1913+16. Six years of accurate measurements of the doubly-peaked radio pulse profile revealed that the flux density in the first component is decreasing relative to the second by ≈ 1 per cent per year, consistent with the line of sight moving across a spot of enhanced emissivity in the magnetosphere at the rate prescribed by geodetic precession. Weisberg et al.'s (1989) upper limit $|\Delta w| < 0°.06$ on the six-year change in pulse width w implies a maximum precession amplitude $\lesssim 0°.4\,\mathrm{yr}^{-1}$, consistent with a relativistic origin and much larger than the predicted radiative precession amplitude of $\approx 0°.001\,\mathrm{yr}^{-1}$. Hence PSR B1913+16 does not usefully constrain the amplitude of radiative precession in old pulsars.

No unambiguous instances of non-relativistic precession are known. Lyne et al. (1988) reported a quasi-sinusoidal variation with a period of ≈ 20 months in the phase residuals of six years of Crab timing data, and a similar feature was claimed to exist in Vela (McCulloch et al. 1990). However, the variation may be an artifact of an unexpectedly high $\ddot{\omega}$ during the exponential relaxation following an overlooked glitch. The quasi-periodic nature of the Vela glitches (Lyne et al. 1996) is also suggestive of precession, but the observed $\dot{\omega}$ as a function of time does not resemble Figure 5. Ulmer (1994) reported that the intensity ratio of the two peaks in the gamma-ray pulse of the Crab seems to vary sinusoidally with a period of $\approx 14\,$yr in both the 50–500 keV and 50 MeV bands (but not in the optical). However, the 14-yr period differs from that observed by Lyne et al. (1988) and a 60 s modulation of the Crab's optical pulses found by Čadež et al. (1997).

Direct measurements of α from pulsar polarization swings do not show any evidence for secular changes on a yearly time-scale. It has been claimed that changes in α on a time-scale of $\sim 10^4\,$yr explain the braking indices of the Crab and Vela, and sudden jumps in α explain the persistent increase in $\dot{\omega}$ following a glitch (Allen & Horvath 1997; Link & Epstein 1997), but the relevant time-scales are too long and too short, respectively, to be precession-related. Tauris & Manchester (1997) used polarization-swing data for more than 100 pulsars to construct the α distribution of the pulsar population, corrected for decreasing beam radius with age. The corrected distribution is skewed towards small α, with $\langle\alpha\rangle$ decreasing on a time-scale of $\approx 10^7\,$yr — once again, too gradual to be a precession-related effect.

The observational evidence against substantial changes in pulse profiles and polarization properties implies that any precession initially present is damped rapidly. Consequently, direct detection of a precessing, isolated pulsar may only be possible in the immediate aftermath of a Galactic supernova. If the precession amplitude is sufficiently large, the newly born pulsar will shine intermittently, as its emission cone drifts into and out of the line of sight, as well as exhibit the profile and polarization changes discussed above.

4.3. Crustal Heating by Internal Friction

Frictional damping inside a neutron star proceeds rapidly in theory. Several authors have estimated the dissipation times due to time-dependent elastic strain (Chau & Henriksen 1971; Macy 1974) and imperfect core-crust coupling (Shaham 1977; de Campli 1980; Alpar & Ögelman 1987; Link et al. 1993) and found them to be small compared to the present ages of young, Crab-like pulsars. (The estimates assume a small precession amplitude; cf. Section 3.) In addition, there is the analogy of friction inside the Earth. Dynamic satellite measurements have revealed that the Earth's non-hydrostatic ellipsoid of inertia has its $\mathbf{e}_3$ axis parallel to $\boldsymbol{\omega}$ to an excellent approximation[5] (Lambeck 1980, p. 31), and that the direction of $\mathbf{e}_3$ fluctuates by less than $1''$ under the action of solar and lunar tides, compared to $\approx 10°$ for the $\mathbf{e}_1$ and $\mathbf{e}_2$ axes (Burša & Pěč 1993, p. 227). Clearly, any drift of $\boldsymbol{\omega}$ away from $\mathbf{e}_3$ is rapidly damped.

In this paper, we are not concerned with the precise origin of the friction in a neutron star; we simply suppose it exists and examine the fate of the dissipated energy. Initially, when the star is precessing, its angular momentum and energy are given by $L_\mathrm{i} = [I_1^2(\omega_{1\mathrm{i}}^2 + \omega_{2\mathrm{i}}^2) + I_3^2\omega_{3\mathrm{i}}^2]^{1/2}$ and $E_\mathrm{i} = \frac{1}{2}I_1(\omega_{1\mathrm{i}}^2 + \omega_{2\mathrm{i}}^2) + \frac{1}{2}I_3\omega_{3\mathrm{i}}^2$. After the precession has been damped, the final angular momentum and energy are given by $L_\mathrm{f} = I_3\omega_{3\mathrm{f}}$ and $E_\mathrm{f} = \frac{1}{2}I_3\omega_{3\mathrm{f}}^2$ ($\boldsymbol{\omega} \to \mathbf{e}_3$ by analogy with the Earth). If the damping occurs over a time τ_d that is short compared to τ_0 and τ_1, we have $L_\mathrm{i} \approx L_\mathrm{f}$ and hence

$$\Delta E = -\tfrac{1}{2}\epsilon I_1(\omega_{1\mathrm{i}}^2 + \omega_{2\mathrm{i}}^2). \tag{27}$$

For $\omega_{1\mathrm{i}} \sim \omega_{2\mathrm{i}} \sim \omega_0$ (Section 3), the total dissipated energy is of order $\epsilon I_1 \omega_0^2$.

We now suppose that the dissipation is localized in the inner and outer crusts, where the ions are organized into a lattice and the shear modulus is non-zero, and we estimate the resulting increase in the star's thermal luminosity L. The thermal conduction time in the crust, τ_cond, is not known with certainty (Nomoto & Tsuruta 1987), so we appeal to the extreme cases of slow cooling ($\tau_\mathrm{d} \ll \tau_\mathrm{cond}$) and fast cooling ($\tau_\mathrm{d} \gg \tau_\mathrm{cond}$) to place bounds on L. In the regime $\tau_\mathrm{d} \ll \tau_\mathrm{cond}$, the dissipated energy ΔE is stored in the crust as heat for a time τ_cond. The crustal heat capacity at a temperature T is given by $c_v \approx 312k_\mathrm{B}(T/\theta_\mathrm{D})^3$ (Shapiro & Teukolsky 1983, p. 100) in the regime where the Debye temperature $\theta_\mathrm{D} \approx 2 \times 10^{10}\,\mathrm{K}$ satisfies

---

[5]I thank P. Goldreich for bringing this fact to my attention.

$T \ll \theta_{\mathrm{D}}$ (i.e. at a density $\rho \approx 1 \times 10^{14}\,\mathrm{g\,cm^{-3}}$). Taking $\Delta E = \epsilon I_1 \omega_0^2$, we find that the final temperature of an iron crust of mass $10^{-3} M$ is $T_{\mathrm{f}} = 2 \times 10^9 (\epsilon \omega_0^2)^{1/4}\,\mathrm{K}$, and its thermal luminosity is $L = 4\pi R^2 \sigma T_{\mathrm{f}}^4 = 1 \times 10^{46} \epsilon \omega_0^2\,\mathrm{erg\,s^{-1}}$. In the opposite regime $\tau_{\mathrm{d}} \gg \tau_{\mathrm{cond}}$, the dissipated heat is conducted rapidly through the crust and one has $L = \Delta E / \tau_{\mathrm{d}} = 1 \times 10^{45} \epsilon \omega_0^2 \tau_{\mathrm{d}}^{-1}\,\mathrm{erg\,s^{-1}}$ (cf. de Campli 1980, p.308), less than the former value for $\tau_{\mathrm{d}} > 0.1\,\mathrm{s}$.

The above estimates imply that the minimum thermal luminosity of a newly born pulsar due to frictional damping of its radiative precession is

$$L \approx 3 \times 10^{31} \left(\frac{\epsilon}{10^{-12}} \right) \left(\frac{\omega}{10^3\,\mathrm{rad\,s^{-1}}} \right)^2 \left(\frac{\tau_{\mathrm{d}}}{1\,\mathrm{yr}} \right)^{-1}\,\mathrm{erg\,s^{-1}} \,. \tag{28}$$

This ought to be detectable given $\tau_{\mathrm{d}} \lesssim 10^{-3}\,\mathrm{yr}$ even if there is significant magnetospheric X-ray emission beamed towards the observer and with $\tau_{\mathrm{d}} \lesssim 3\,\mathrm{yr}$ if there is not. The duration of the thermal source is the maximum of τ_{d} and τ_{cond}, starting from the time when the star first crystallizes into a body with a rigid crust spinning down electromagnetically. If the crystallization epoch occurs very shortly after the supernova explosion itself, it may not be possible to detect L at all.

5. CONCLUSION

In this paper, the rotation of a rigid, aspherical, internally frictionless neutron star is analyzed. We show that, in general, the free precession period τ_2 due to elastic and magnetic deformations is comparable to the radiative precession period τ_1 associated with the near-field component of the radiation torque. In other words, the 'free' precession is not truly free, a fact that has been overlooked in the literature to date.

In the regime $\tau_1 \sim \tau_2$, the star rotates in a distinctive way: (i) it precesses and nutates anharmonically, typically with an amplitude of tens of degrees (Section 3.2); (ii) the magnetic inclination angle α swings through tens of degrees during one precession period (Section 3.3); (iii) the precession can persist or decay to zero (i.e. steady rotation) depending on the parameters β and χ and the initial orientation of $\boldsymbol{\omega}$ (Section 3.4); and (iv) the frequency derivative $\dot{\omega} < 0$ oscillates about its overall spin-down trend, exhibiting spiky, glitch-like behaviour for triaxial stars with $\epsilon \tau_1 \approx \epsilon' \tau_2$ (Section 3.5).

The precession and nutation lead to fractional changes of order unity in the pulse profile, polarization swing and $\dot{\omega}$ of an isolated pulsar on a time-scale $\sim x_0 \tau_0 \ll \tau_0$, with $x_0 \tau_0 \approx 10\,\mathrm{yr}$ for young, Crab-like objects and $x_0 \tau_0 \approx 10^3\,\mathrm{yr}$ for old pulsars. Such changes are not observed. One plausible explanation is that a young neutron star has $\boldsymbol{\omega}$ parallel to $\mathbf{e}_3$ when its crust crystallizes shortly after birth — but this is not true for neutron stars with large hydromagnetic deformations, given current viscosity estimates (Section 4.1). Another explanation is that the precession and nutation are damped by internal friction, perhaps due to time-dependent elastic strains in the crust. If the damping takes place over a time τ_{d}, we show (Section 4.3) that the dissipated energy

$\Delta E \approx \epsilon I_1 \omega_0^2$ either heats the crust to a temperature $T_{\rm f} = 2 \times 10^9 (\epsilon \omega_0^2)^{1/4}$ K for $\tau_{\rm d} \ll \tau_{\rm cond}$, yielding a thermal X-ray luminosity $L = 1 \times 10^{46} \epsilon \omega_0^2 \, {\rm erg \, s^{-1}}$, or else is conducted rapidly to the surface, yielding $L = 1 \times 10^{45} \epsilon \omega_0^2 \tau_{\rm d}^{-1} \, {\rm erg \, s^{-1}}$. The luminosity L may be detectable depending on how soon after the supernova explosion the neutron-star crust crystallizes, and the intensity of magnetospheric X-ray emission at that epoch.

REFERENCES

Abney M., Epstein R. I., Olinto A. V., 1996, ApJ, 466, L91

Allen M. P., Horvath J. E., 1997, MNRAS, 287, 615

Alpar A., Ögelman H., 1987, A&A, 185, 196

Arons J., 1998, in Shibazaki N., Kawai N., Shibata S., Kifune T., eds, Neutron Stars and Pulsars, Universal Academy Press, Tokyo, p. 339

Blandford R. D., Applegate J. H., Hernquist L., 1983, MNRAS, 204, 1025

Burša M., Pěč K., 1993, Gravity Field and Dynamics of the Earth, Springer-Verlag, Berlin

Čadež A., Galičič M., Calvani M., 1997, A&A, 324, 1005

Casini H., Montemayor R., 1998, ApJ, 503, 374

Chau W. Y., Henriksen R. N., 1971, Astrophys. Lett., 8, 49

Cutler C., Lindblom L., 1987, ApJ, 314, 234

Davis L., Goldstein M., 1970, ApJ, 159, L81

de Campli W. M., 1980, ApJ, 242, 306

Deutsch A. J., 1955, Ann. d'Astrophysique, 18, 1

Easson I., 1979, ApJ, 233, 711

Goldreich P., 1970, ApJ, 160, L11

Good M. L., Ng K. K., 1985, ApJ, 299, 706

Haensel P., Urpin V. A., Yakovlev D. G., 1990, A&A, 229, 133

Kaburaki O., 1981, Ap&SS, 74, 333

Lambeck K., 1980, The Earth's Variable Rotation: Geophysical Causes and Consequences, Cambridge Univ. Press, Cambridge

Link B., Epstein R. I., Baym G., 1993, ApJ, 403, 285

Link B., Epstein R. I., 1997, ApJ, 478, L91

Lyne A. G., Pritchard R. S., Smith F. G., 1988, MNRAS, 233, 667

Lyne A. G., Pritchard R. S., Smith F. G., Camilo F., 1996, Nature, 381, 497

Macy W. W., 1974, ApJ, 190, 153

McCulloch P. M., Hamilton P. A., McConnell D., King E. A., 1990, Nature, 346, 822

Melatos A., 1997, MNRAS, 288, 1049

Muslimov A., Page D., 1996, ApJ, 458, 347

Nomoto K., Tsuruta S., 1987, ApJ, 312, 711

Pal S., Bandyopadhyay D., Chakrabarty S., 1998, astro-ph/9806356

Sedrakian A., Wasserman I., Cordes J. M., 1998, astro-ph/9801188

Shaham J., 1977, ApJ, 214, 251

Shapiro S. L., Teukolsky S. A., 1983, Black Holes, White Dwarfs, and Neutron Stars: The Physics of Compact Objects, Wiley, New York

Tauris T. M., Manchester R. N., 1998, MNRAS, 298, 625

Thompson C., Duncan R. C., 1993, ApJ, 408, 194

Ulmer M. P. et al., 1994, ApJ, 432, 228

Weisberg J. M., Romani, R. W., Taylor, J. H., 1989, ApJ, 347, 1030

Yuan Y. F., Zhang J. L., 1998, A&A, 335, 969

A.   DERIVATION OF EULER'S EQUATIONS

We ignore the slight distortion of the star from a perfectly spherical figure when calculating its radiation fields and the radiation-reaction torque. The electromagnetic fields $\mathbf{E}(\mathbf{x}, t)$ and $\mathbf{B}(\mathbf{x}, t)$ generated by a magnetized, conducting sphere rotating *in vacuo* were derived using a multipole method by Deutsch (1955) and subsequently corrected for minor typographical errors by Melatos (1997); see also Kaburaki (1981). The radiation torque exerted on the rotating sphere can be calculated from $\mathbf{E}(\mathbf{x}, t)$ and $\mathbf{B}(\mathbf{x}, t)$ by integrating the angular momentum flux vector over any surface S enclosing the sphere:

$$\mathbf{N} = \varepsilon_0 \int_S \left[(\mathbf{x} \times \mathbf{E})\,\mathbf{E} \cdot d\mathbf{S} + c^2 (\mathbf{x} \times \mathbf{B})\,\mathbf{B} \cdot d\mathbf{S} - \tfrac{1}{2}(E^2 + c^2 B^2)(\mathbf{x} \times d\mathbf{S}) \right] \ . \tag{A1}$$

Let the radius of the sphere be r_0, let its angular frequency be ω, let α denote the angle between its rotation and magnetic axes, and assume that the frozen-in magnetic field is dipolar, with polar magnitude B_0. Then, in a Cartesian coordinate system (x, y, z) where the z axis is oriented along the instantaneous rotation axis $\boldsymbol{\omega}$ and the magnetic axis $\mathbf{m}$ simultaneously lies in the x-z plane, the instantaneous radiation torque assumes the form

$$(N_x, N_y, N_z) = \frac{2\pi B_0^2 r_0^6 \omega^3}{\mu_0 c^3} \left[\sin\alpha \cos\alpha F(x_0), \sin\alpha \cos\alpha G(x_0), -\sin^2\alpha F(x_0) \right] \ , \tag{A2}$$

with

$$F(x_0) = \frac{x_0^4}{5(x_0^6 - 3x_0^4 + 36)} + \frac{1}{3(x_0^2 + 1)}, \tag{A3}$$

$$G(x_0) = \frac{3(x_0^2 + 6)}{5x_0(x_0^6 - 3x_0^4 + 36)} + \frac{3 - 2x_0^2}{15x_0(x_0^2 + 1)}. \tag{A4}$$

Strictly speaking, it is incorrect to refer to (A2) as an instantaneous torque, because it is calculated under the assumption that the star has been rotating, and will continue to rotate, at a constant angular frequency ω; formally, it is assumed that the radiation fields exist for all t and are proportional to $e^{i\omega t}$, as for an infinitely massive star. However, the approximation is an excellent one for a neutron star, where the braking and precession time-scales τ_0, τ_1, τ_2 (Sections 2.2, 2.3) satisfy $\tau_0, \tau_1, \tau_2 \gg \omega^{-1}$.

The form factors (A3) and (A4) differ from the expressions $F(x_0) = 1/3$ and $G(x_0) = 1/2x_0$ appearing in previous works (Davis & Goldstein 1970; Goldreich 1970). There are two reasons for this difference: (i) previous authors only included terms of leading order in the small parameter x_0 (cf. Section 3.6), whereas (A3) and (A4) are exact for arbitrary x_0; and (ii) previous authors modelled the star as a sphere of uniform internal magnetization, whereas in this paper the star is modelled as a perfectly conducting sphere with a point magnetic dipole at its centre (Deutsch 1955), affecting the polynomial coefficients in (A3) and (A4).

The Cartesian coordinate system (x, y, z) rotates with respect to the star as $\boldsymbol{\omega}$ changes orientation under the action of $\mathbf{N}$. Among other things, this causes α to change with time. In

order to write down Euler's equations, it is necessary to reexpress $\mathbf{N}$ in body coordinates that are fixed with respect to the star. We choose the body axes to be the principal axes of the star's ellipsoid of inertia, $\mathbf{e}_1$, $\mathbf{e}_2$ and $\mathbf{e}_3$; the magnetic axis $\mathbf{m}$, which is also fixed with respect to the star, is taken to lie in the plane spanned by $\mathbf{e}_1$ and $\mathbf{e}_3$, at an angle χ to $\mathbf{e}_3$ (a slight loss of generality). The transformation from (x, y, z) to body coordinates is time-dependent, but it is not an Euler transformation because (x, y, z) is a non-inertial frame. It is described by a matrix $[A_{ij}]$, defined through $(\mathbf{e}_1, \mathbf{e}_2, \mathbf{e}_3) = [A_{ij}] \cdot (\mathbf{i}, \mathbf{j}, \mathbf{k})$, which can be represented in the form

$$[A_{ij}] = \begin{pmatrix} \cos\phi\cos\theta\cos\psi - \sin\phi\sin\psi & \sin\phi\cos\theta\cos\psi + \cos\phi\sin\psi & -\sin\theta\cos\psi \\ -\cos\phi\cos\theta\sin\psi - \sin\phi\cos\psi & -\sin\phi\cos\theta\sin\psi + \cos\phi\cos\psi & \sin\theta\sin\psi \\ \cos\phi\sin\theta & \sin\phi\sin\theta & \cos\theta \end{pmatrix}, \quad \text{(A5)}$$

where the angles ϕ, ψ, θ (*not* Euler angles) depend on t through the principal angular velocity components ω_1, ω_2, ω_3 as follows:

$$\cos\phi = \frac{\omega\cos\chi - \omega_3\cos\alpha}{\sin\alpha(\omega^2 - \omega_3^2)^{1/2}}, \quad \text{(A6)}$$

$$\sin\phi = -\frac{\omega_2\sin\chi}{\sin\alpha(\omega^2 - \omega_3^2)^{1/2}}, \quad \text{(A7)}$$

$$\cos\psi = -\frac{\omega_1}{(\omega^2 - \omega_3^2)^{1/2}}, \quad \text{(A8)}$$

$$\sin\psi = \frac{\omega_2}{(\omega^2 - \omega_3^2)^{1/2}}, \quad \text{(A9)}$$

$$\cos\theta = \omega_3/\omega, \quad \text{(A10)}$$

$$\sin\theta = (1 - \omega_3^2/\omega^2)^{1/2}. \quad \text{(A11)}$$

The angle α is chosen to lie in the range $0 \leq \alpha \leq \pi$ and satisfies

$$\omega\cos\alpha = \omega_1\sin\chi + \omega_3\cos\chi. \quad \text{(A12)}$$

Upon substituting (A6) to (A12) into (A5) and employing the relation $(N_1, N_2, N_3) = [A_{ij}] \cdot (N_x, N_y, N_z)$, we arrive at the principal components of the radiation torque featured on the right-hand sides of Euler's equations (1), (2) and (3).

B.   APPROXIMATE ANALYTIC SOLUTION FOR $\epsilon' = 0$, $\chi = 90°$

In this appendix, we derive an approximate solution to Euler's equations (1), (2) and (3) for a biaxial star ($\epsilon' = 0$) with $\chi = 90°$. The solution is accurate provided the precession periods τ_1 (radiative) and τ_2 (free) are much smaller than the braking time-scale τ_0.

When the slow braking terms, proportional to $(\omega_0\tau_0)^{-1}F(x_0)$, are neglected relative to the fast precessive terms, proportional to ϵ and $(\omega_0\tau_0)^{-1}uG(x_0)$, Euler's equations reduce to the

zeroth-order system (15) to (17) which, in the special case $\chi = 90°$, reduces to

$$\dot{u}_1 = -\epsilon u_2 u_3 , \tag{B1}$$

$$\dot{u}_2 = \epsilon(1 + \beta^{-1})u_1 u_3 , \tag{B2}$$

$$\dot{u}_3 = -\epsilon\beta^{-1}u_1 u_2 . \tag{B3}$$

The solutions of (B1) to (B3) are Jacobian elliptic functions. The relative signs of the coefficients on the right-hand sides determine the solution branch, given the physical requirement that u_1, u_2 and u_3 are real quantities whose squared amplitudes are non-negative. We distinguish three solution branches:

Case I: $\beta > 0$.

$$u_1 = \left(\frac{\gamma + \eta\beta}{\beta + 1}\right)^{1/2} \mathrm{cn}\left[\epsilon\left(\frac{\eta - \gamma}{\beta}\right)^{1/2} s + \Phi\right], \tag{B4}$$

$$u_2 = \left(\frac{\gamma + \eta\beta}{\beta}\right)^{1/2} \mathrm{sn}\left[\epsilon\left(\frac{\eta - \gamma}{\beta}\right)^{1/2} s + \Phi\right], \tag{B5}$$

$$u_3 = \left(\frac{\eta - \gamma}{\beta + 1}\right)^{1/2} \mathrm{dn}\left[\epsilon\left(\frac{\eta - \gamma}{\beta}\right)^{1/2} s + \Phi\right], \tag{B6}$$

$$k^2 = \frac{\gamma + \eta\beta}{\beta(\eta - \gamma)} . \tag{B7}$$

Case II: $-1 < \beta < 0$.

$$u_1 = \gamma^{1/2}\mathrm{cn}\left[\epsilon\left(\frac{\eta - \gamma}{-\beta}\right)^{1/2} s + \Phi\right], \tag{B8}$$

$$u_2 = (\eta - \gamma)^{1/2}\mathrm{dn}\left[\epsilon\left(\frac{\eta - \gamma}{-\beta}\right)^{1/2} s + \Phi\right], \tag{B9}$$

$$u_3 = \left(\frac{\gamma}{-\beta}\right)^{1/2} \mathrm{sn}\left[\epsilon\left(\frac{\eta - \gamma}{-\beta}\right)^{1/2} s + \Phi\right], \tag{B10}$$

$$k^2 = -\frac{(\beta + 1)\gamma}{\beta(\eta - \gamma)} . \tag{B11}$$

Case III: $\beta < -1$.

$$u_1 = \left(\frac{\gamma + \eta\beta}{\beta + 1}\right)^{1/2} \mathrm{sn}\left[-\epsilon\left(\frac{\beta + 1}{\beta}\right)^{1/2}\left(\frac{\gamma}{-\beta}\right)^{1/2} s + \Phi\right], \tag{B12}$$

$$u_2 = \left(\frac{\gamma + \eta\beta}{\beta}\right)^{1/2} \mathrm{cn}\left[-\epsilon\left(\frac{\beta + 1}{\beta}\right)^{1/2}\left(\frac{\gamma}{-\beta}\right)^{1/2} s + \Phi\right], \tag{B13}$$

$$u_3 = \left(\frac{\gamma}{-\beta}\right)^{1/2} \mathrm{dn}\left[-\epsilon\left(\frac{\beta + 1}{\beta}\right)^{1/2}\left(\frac{\gamma}{-\beta}\right)^{1/2} s + \Phi\right], \tag{B14}$$

$$k^2 = \frac{\gamma + \eta\beta}{(\beta + 1)\gamma} . \tag{B15}$$

In (B4) to (B15), the quantities η, γ and Φ are all constants of the motion (see Section 2.4). The trivial cases $\beta = -1$ (harmonic precession about $\mathbf{e}_2$) and $\beta = 0$ (spherical star; see Davis & Goldstein 1970) are not treated here.

When terms proportional to $(\omega_0\tau_0)^{-1}F(x_0)$ are restored to Euler's equations, the above solutions remain approximately valid, but the constants of the motion are converted into slowly varying functions of s. We now compute the slow evolution of $\eta(s)$, $\gamma(s)$ and $\Phi(s)$. First, we substitute (B4) to (B15) into (1), (2) and (3) and perform the time derivatives explicitly. For each solution branch, this results in a system of three equations linear in $\dot\eta$, $\dot\gamma$ and $\dot\Phi$. For example, the $\beta > 0$ branch yields

$$\frac{\dot\gamma + \dot\eta\beta}{2(\gamma + \eta\beta)} = -\frac{F(x_0)\eta}{\omega_0\tau_0}\,\mathrm{sn}^2 \ , \tag{B16}$$

$$\left[\epsilon\left(\frac{\beta}{\eta - \gamma}\right)^{1/2}\frac{\dot\eta - \dot\gamma}{2\beta}s + \dot\Phi\right]\mathrm{dn}^2 = -\frac{F(x_0)\eta}{\omega_0\tau_0}\,\mathrm{sn\,cn\,dn} \ , \tag{B17}$$

$$-\frac{\dot\gamma + \dot\eta\beta}{2\beta(\eta - \gamma)}\,\mathrm{cn}^2 + \frac{\dot\eta - \dot\gamma}{2(\eta - \gamma)}\,\mathrm{dn}^2 = -\frac{F(x_0)\eta}{(1 + \epsilon)\omega_0\tau_0}\,\mathrm{dn}^2 + \frac{\epsilon^2(\gamma + \eta\beta)}{(1 + \epsilon)\beta^{3/2}(\eta - \gamma)^{1/2}}\,\mathrm{sn\,cn\,dn} \ . \tag{B18}$$

In (B16) to (B18), Euler's equations are linearly combined in such a way that the coefficients of $\dot\eta$, $\dot\gamma$ and $\dot\Phi$ are squares of elliptic functions, in order to ensure a non-trivial result when averaging over Φ. The (omitted) arguments of the elliptic functions are the same as in (B4) to (B6). We now average over Φ, holding constant η, γ, and their derivatives. The results for the three solution branches are as follows:

Case I: $\beta > 0$.

$$\dot\eta = -\frac{2F(x_0)\eta[(1 + \epsilon)(\gamma + \eta\beta)I_1(I_2 + \beta I_3) + \beta(\eta - \gamma)I_3]}{\omega_0\tau_0(1 + \epsilon)\beta(\beta + 1)I_3} \ , \tag{B19}$$

$$\dot\gamma = \frac{2F(x_0)\eta[(1 + \epsilon)(\gamma + \eta\beta)I_1(I_2 - I_3) + \beta(\eta - \gamma)I_3]}{\omega_0\tau_0(1 + \epsilon)(\beta + 1)I_3} \ , \tag{B20}$$

$$\dot\Phi = \frac{F(x_0)\eta[(1 + \epsilon)(\gamma + \eta\beta)I_1 I_2 + \beta(\eta - \gamma)I_3]}{\omega_0\tau_0(1 + \epsilon)\beta^2 I_3}\left(\frac{\beta}{\eta - \gamma}\right)^{1/2}\epsilon s \ . \tag{B21}$$

Case II: $-1 < \beta < 0$.

$$\dot\eta = -\frac{2F(x_0)\eta\{(1 + \epsilon)\beta(\eta - \gamma)I_3 + \gamma I_1[\beta I_3 - (\beta + 1)I_2]\}}{\omega_0\tau_0(1 + \epsilon)\beta I_3} \ , \tag{B22}$$

$$\dot\gamma = -\frac{2F(x_0)\eta\gamma I_1}{\omega_0\tau_0(1 + \epsilon)} \ , \tag{B23}$$

$$\dot\Phi = \frac{\epsilon^2 I_4}{(1 + \epsilon)I_3}\left(\frac{\eta - \gamma}{-\beta}\right)^{1/2} - \frac{F(x_0)\eta[(1 + \epsilon)\beta(\eta - \gamma)I_3 - (\beta + 1)\gamma I_1 I_2]}{\omega_0\tau_0(1 + \epsilon)\beta^2 I_3}\left(\frac{-\beta}{\eta - \gamma}\right)^{1/2}\epsilon s \ . \tag{B24}$$

Case III: $\beta < -1$.

$$\dot\eta = -\frac{2F(x_0)\eta\{(1 + \epsilon)(\gamma + \eta\beta)I_2[(\beta + 1)I_3 + I_1] - (\beta + 1)\gamma I_3\}}{\omega_0\tau_0(1 + \epsilon)\beta(\beta + 1)I_3} \ , \tag{B25}$$

$$\dot{\gamma} = -\frac{2F(x_0)\eta[-(1+\epsilon)(\gamma+\eta\beta)I_1 I_2 + (\beta+1)\gamma I_3]}{\omega_0 \tau_0 (1+\epsilon)(\beta+1)I_3} \ , \tag{B26}$$

$$\dot{\Phi} = \frac{F(x_0)\eta[-(1+\epsilon)(\gamma+\eta\beta)I_1 I_2 + (\beta+1)\gamma I_3]}{\omega_0 \tau_0 (1+\epsilon)\beta(\beta+1)I_3} \left(\frac{\beta+1}{-\gamma}\right)^{1/2} \epsilon s \ . \tag{B27}$$

In (B19) to (B27), the Φ averages I_i ($1 \le i \le 4$) are all functions of the modulus k appropriate for each branch and are defined by $I_1 = \langle \mathrm{sn}^2\Phi \rangle$, $I_2 = \langle \mathrm{cn}^2\Phi \rangle$, $I_3 = \langle \mathrm{dn}^2\Phi \rangle$, and $I_4 = \langle \mathrm{cn}^2\Phi\,\mathrm{dn}^2\Phi \rangle$.

In the limit $\beta \to \infty$ (i.e. $k \to 0$), the three solution branches merge together into one, the elliptic functions reduce to trigonometric functions, and the equations for $\dot{\eta}$, $\dot{\gamma}$, $\dot{\Phi}$ reduce to those given by Goldreich (1970).
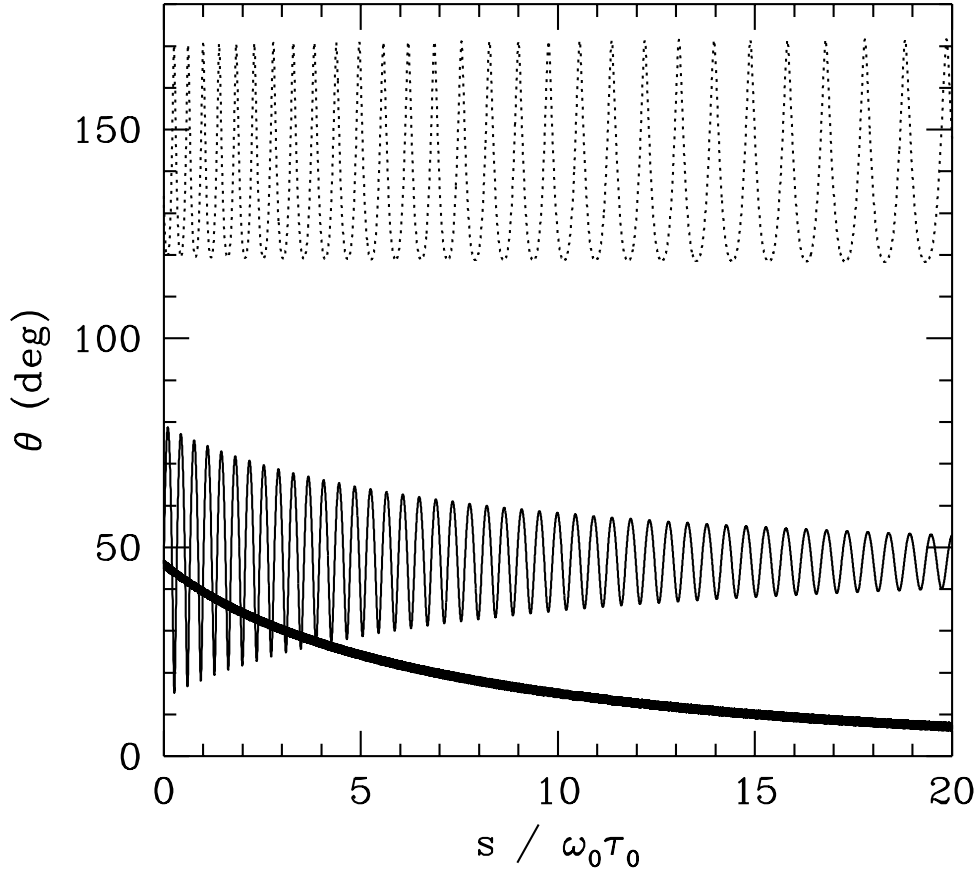
Fig. 1.— Precession angle θ, in degrees, as a function of time, in units of the spin-down time-scale τ_0. Thick band: $\beta = 20$, $\chi = 20°$, $uG(x_0) = 47.4$, $u_{1,0} = 0.387$, $u_{2,0} = 0.6$, $u_{3,0} = 0.7$. Although not apparent to the eye, the band is a rapid oscillation with a peak-to-peak amplitude of $\approx 1.6°$. Solid curve: $\beta = 0.8$, $\chi = 20°$, $uG(x_0) = 47.4$, $u_{1,0} = 0.387$, $u_{2,0} = 0.6$, $u_{3,0} = 0.7$. Dotted curve: $\beta = 0.8$, $\chi = 20°$, $uG(x_0) = 47.4$, $u_{1,0} = 0.387$, $u_{2,0} = 0.6$, $u_{3,0} = -0.7$.
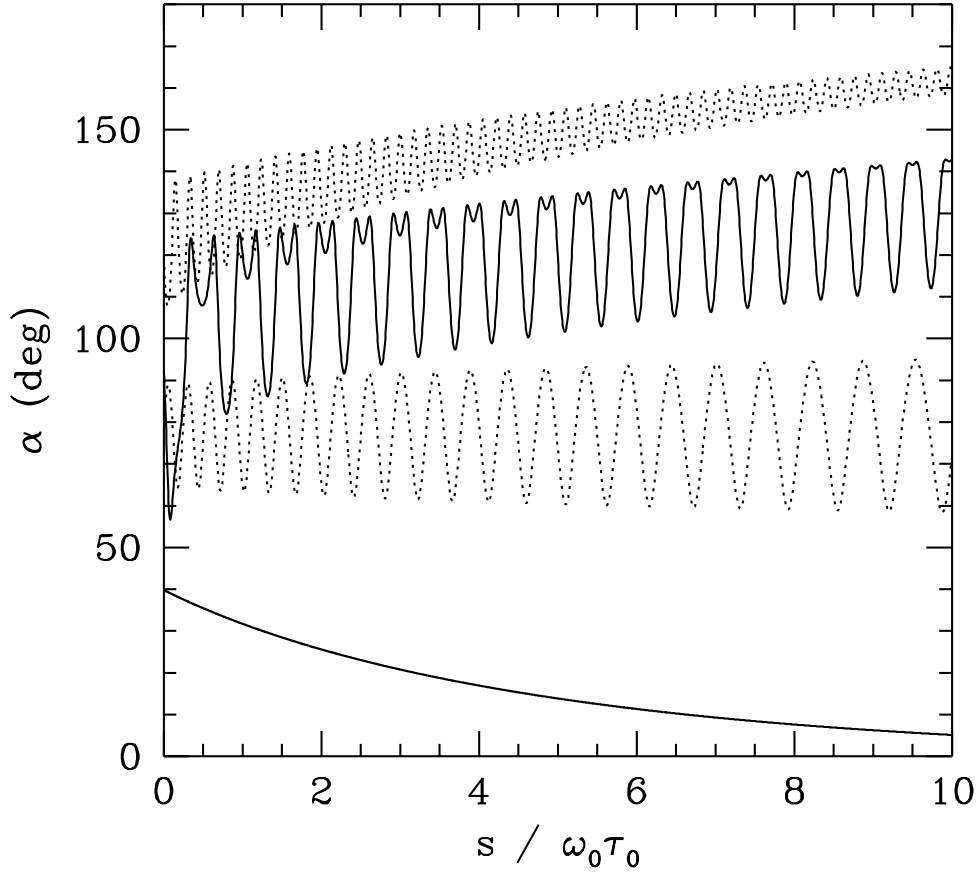
Fig. 2.— Magnetic inclination angle α, in degrees, as a function of time, in units of the spin-down time-scale τ_0, for $uG(x_0) = 47.4$ and initial conditions $u_{1,0} = -0.5$, $u_{2,0} = 0.4$, $u_{3,0} = 0.768$. Lower solid curve: $\beta = 0.5$, $\chi = 0°$. Lower dotted curve: $\beta = 0.5$, $\chi = 45°$. Upper solid curve: $\beta = -0.5$, $\chi = 60°$. Upper dotted curve: $\beta = -0.5$, $\chi = 90°$.
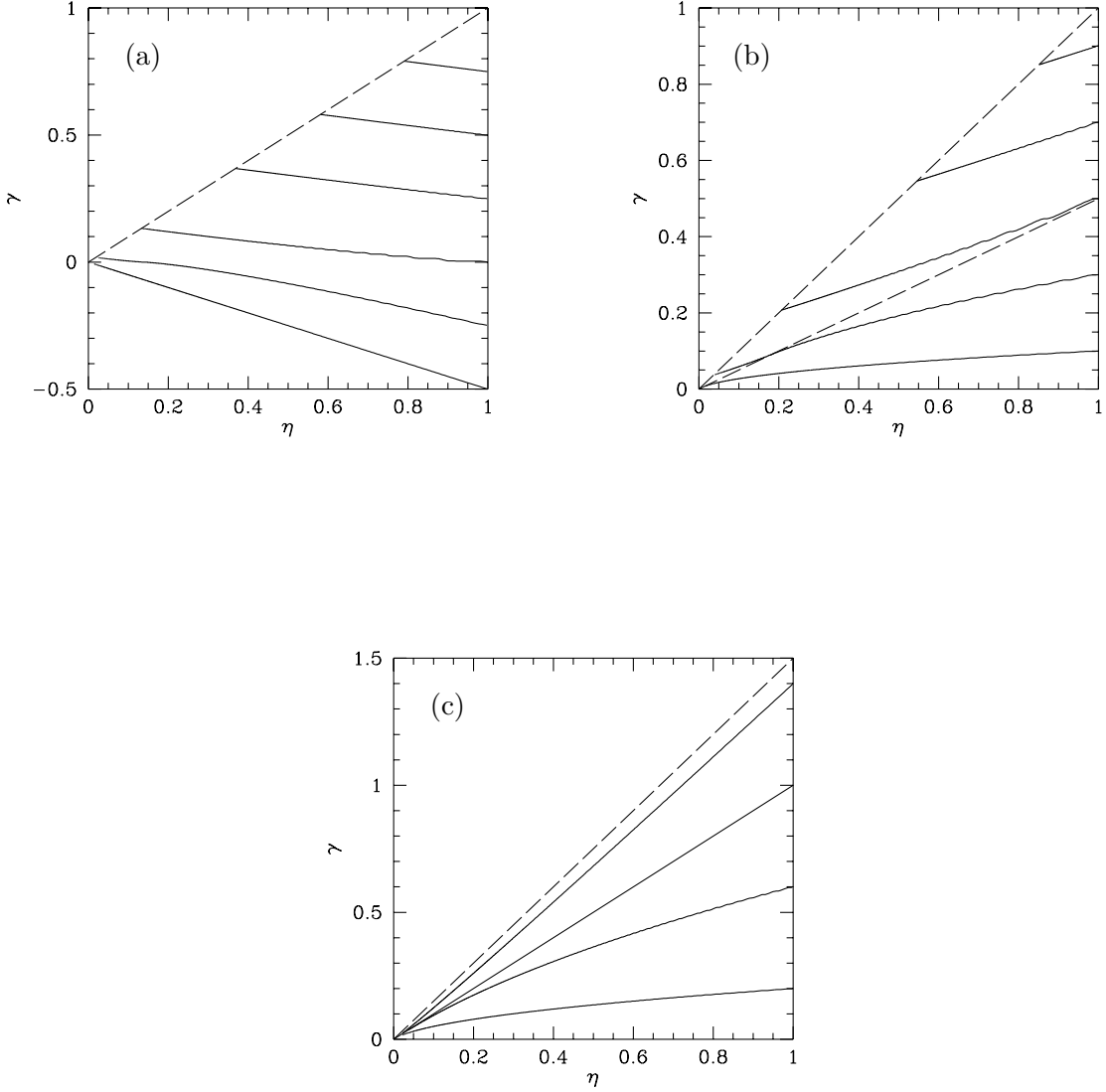
Fig. 3.— Phase diagrams showing trajectories in the η-γ plane, for $uG(x_0) = 47.4$, $\chi = 90°$, and $0 \le s \le 10^2\omega_0\tau_0$. The trajectories begin at $\eta = 1$, with different initial values of γ corresponding to different initial conditions, and move from right to left across the diagrams. The broken diagonals are the lines $\eta = \gamma$ and $\eta = -\beta\gamma$. Phase diagrams are shown for three stars: (a) $\beta = 0.5$ (oblate), (b) $\beta = -0.5$ (prolate), (c) $\beta = -1.5$ (prolate).
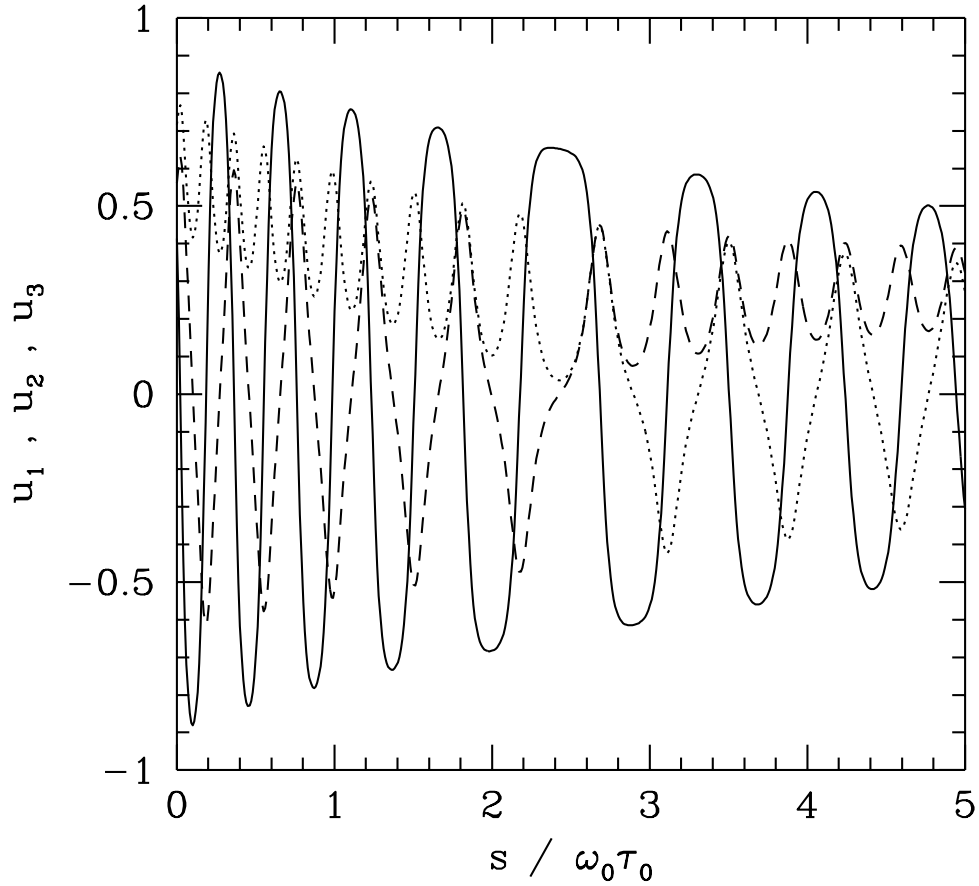
Fig. 4.— Principal angular frequency components u_1 (dashed curve), u_2 (dotted curve) and u_3 (solid curve), in units of ω_0, as functions of time, in units of the spin-down time-scale τ_0. Note that u_1 and u_2 interchange oscillation modes at $s \approx 2.7\,\omega_0\tau_0$. All curves are for $\chi = 90°$, $\beta = -0.5$, $uG(x_0) = 47.4$, $u_{1,0} = 0.539$, $u_{2,0} = 0.7$, $u_{3,0} = 0.469$.
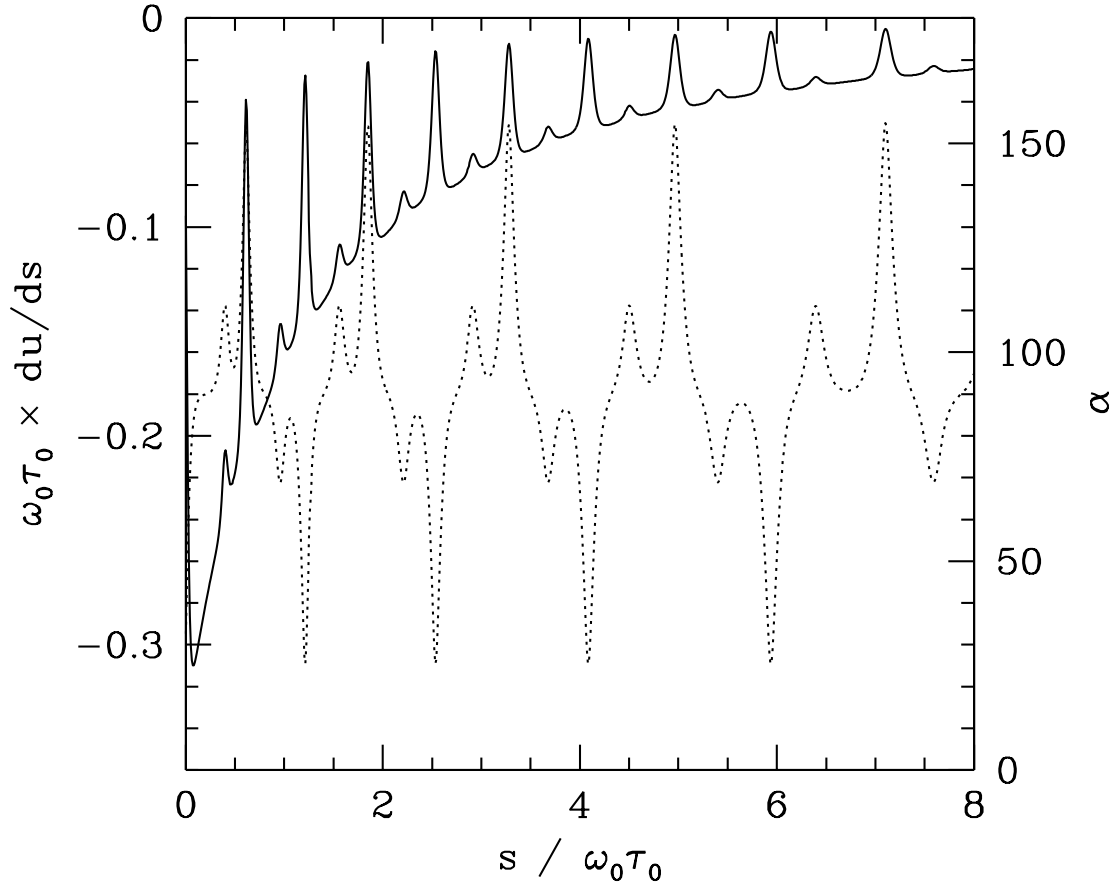
Fig. 5.— Angular frequency derivative $\dot{u}$ (solid curve), in units of $(\omega_0\tau_0)^{-1}$, and magnetic inclination angle α (dotted curve), in degrees, as functions of time, in units of the braking time-scale τ_0. The local minima and maxima of $\dot{u}$ and α correspond one-to-one. Both curves are for $\chi = 40°$, $\beta = 9.5$, $\epsilon' = 0.09\epsilon$, $uG(x_0) = 9.8$, $u_{1,0} = 0.873$, $u_{2,0} = 0.28$, $u_{3,0} = 0.4$.